Journal of Computers Vol. 37 No. 5, October 2026, pp. 75-88
https://doi.org/10.63367/19911599202610370500 6

Research on Scheduling Strategy of Wind-Solar-Thermal-Storage System Based on MNSGA-II

Yun Wu[1], Kai Yang[1*], Yan Du[2], Jie-Ming Yang[1], Zi-Yi Wang[1], Ning An[3], Nan Xu[3], and Wen-Han Zhao[1]

[1] School of Computer Science, Northeast Electric Power University,
Jilin 132012, China
838558160@qq.com, 2639191106@qq.com, yjmlzy@sina.com,
2500704196@qq.com, 2638493792@qq.com

[2] Jilin Meteorological Observation and Protection Center, Jilin Meteorological Service,
Changchun 130000, China
1072302536@qq.com

[3] Northeast Branch of State Grid Corporation of China,
Shenyang 110180, China
13555825869@163.com, 13704032140@139.com

Received 22 July 2025; Revised 6 February 2026; Accepted 13 February 2026

Abstract. This paper proposes an improved NSGA-II algorithm (MNSGA-II) to address the issues of local optima and insufficient population diversity in the process of solving economic dispatch strategies for power systems. The algorithm first uses Faure sequences to initialize the population, improving the quality and distribution uniformity of the initial solution; Secondly, design a dual archive maintenance strategy that updates the convergence archive through PBI values, updates the diversity archive through Manhattan distance, and combines truncation mechanism to prevent archive overflow, enhancing the algorithm's global search capability. In the process of evolution, combining two archive information for environmental selection balances convergence and diversity. The application of MNSGA-II to the power scheduling problem of four generator units shows that compared with traditional NSGA-II and its variants, the algorithm proposed in this paper performs better in terms of optimization accuracy and stability, providing an effective solution for multi-objective optimization of power systems under complex constraints.

keywords: wind-solar-thermal-storage system, NSGA-II, scheduling strategy

1 Introduction

In recent years, driven by policy support and capital investment, clean energy sources such as wind power and photovoltaic have developed rapidly. With the iterative technological upgrades, the efficiency of new energy generation has significantly improved, and its share in the power system has continued to expand. However, the inherent intermittency and volatility of these energy sources pose new challenges to the stable operation of the power grid. Against this backdrop, modern thermal power units with deep peak shaving capabilities, due to their outstanding power supply stability, remain a crucial support for ensuring the reliable operation of the power grid. Meanwhile, breakthroughs have been made in energy storage technology, with various technical routes from lithium batteries to flow batteries achieving large-scale application, providing key solutions for flexible regulation in the power system.

Power system optimal dispatch is a complex multi-objective optimization problem with nonlinearity, strong constraints, and multiple peaks. In recent years, researchers have proposed various innovative solutions. Wang et al. [1] proposed an optimal dispatch model considering demand response for the integration of new energy generation. They improved the Harris hawks optimization (HHO) algorithm to address the issues of uneven population distribution and easy trapping in local optima. By introducing the Tent mapping in the initialization stage and the Levy flight function in the search stage, the effectiveness of the proposed strategy was verified through experiments. Zhu et al. [2] addressed the issue of wasted wind and solar energy in the power system

* Corresponding Author

by adding a hydrogen production system and a hydrogen fuel cell system to the traditional wind-solar-thermal power generation system. They established a new power system dispatch model that converts excess wind and solar energy into hydrogen. Additionally, they proposed a new crowding distance calculation method based on variance to address the crowding degree of the NSGA-II algorithm, and verified the improved algorithm's enhanced distribution and convergence through test functions. Simulation results demonstrated the effectiveness of the proposed power dispatch model and the improved algorithm in solving the economic dispatch problem of the power system. Wang et al. [3] constructed a multi-objective capacity optimization model aiming to minimize operating costs, maximize the proportion of renewable energy consumption, and minimize the system's comprehensive cost. They combined reverse learning, artificial bee colony, dynamic reverse, and whale optimization strategies in the bee colony optimization (BWO) algorithm to enhance population diversity and convergence accuracy, ultimately improving the algorithm's optimization performance. Guan et al. [4] proposed a multi-objective optimization dispatch model under grid-connected mode that comprehensively considers the economic operation cost and environmental protection cost of the power system. They utilized a particle swarm optimization model with the introduction of inertia factors and adaptive particle mutation for solution. Despite the continuous emergence of various novel algorithms, NSGA-II remains the widely recognized benchmark in the field of multi-objective optimization [5], thanks to the robustness of its non-dominated sorting, its relative advantage in computational complexity, and its exceptional framework versatility. For instance, Hazra et al. [6] applied NSGA-II to Multi-Area Economic and Emission Dispatch (MAEED). By synergistically optimizing operating costs and environmental emissions, their work provides effective support for sustainable decision-making in power system operations.

Based on this, this study proposes an improved NSGA-II algorithm (MNSGA-II). This algorithm integrates a population initialization strategy based on Faure sequences and a dual archive maintenance mechanism: Firstly, it uses Faure sequences to generate a high-quality initial population, ensuring a good distribution of the initial solutions; secondly, it maintains convergence and diversity archives based on PBI values and Manhattan distances respectively through solution space partitioning, and employs an intelligent truncation mechanism to prevent archive overflow. During the evolutionary process, the algorithm collaboratively utilizes the information from the two archives for environmental selection, ensuring both convergence and maintenance of population diversity. Finally, the improved algorithm is applied to solve the multi-objective scheduling model of the power system, providing an optimized scheduling strategy for system operation. The subsequent structure of this paper is organized as follows: Section 2 constructs a multi-objective dispatch mathematical model for the wind-solar--thermal-storage system. Section 3 elaborates on the improved MNSGA-II algorithm. Section 4 conducts an experimental simulation analysis, validating the advantages of MNSGA-II in dispatch accuracy and stability through comparisons with multiple algorithms.

2 Mathematical Model for Scheduling

To achieve the synergistic optimization of economy and safety, a scheduling mathematical model based on a multi-objective optimization framework is constructed. The model includes objective functions and constraints, which are specifically defined as follows [7].

2.1 Objective Functions

The objective functions defined in this section include economic operation costs and an energy storage health evaluation function.

Economic Operating Costs. The economic operation costs comprise the operational costs of generation units and the utilization costs of renewable energy. For unit operation costs C_a, the optimization objective is to minimize the operating and maintenance costs of the unit, and the calculation method is shown in formula (1):

$$C_a = \sum_{t=1}^{T} \sum_{i=1}^{N} (C_{i,f} P_i(t) + C_{i,m} P_i(t) \tag{1}$$

In the formula: t is the scheduling period number, and within one scheduling period, the running parameters remain unchanged; T is the number of scheduling periods within one scheduling cycle; i is the serial number of the steam turbine unit; N is the number of steam turbines; $C_{i,f}$ is the i-th turbine fuel cost coefficient, and $C_{i,m}$ is the i-th turbine maintenance cost coefficient; $P_i(t)$ is the power generation of the i-th turbine during the t-th scheduling period.

The utilization costs of renewable energy C_b is shown in formula (2):

$$C_b = \sum_{t=1}^{T} C_E P_{Euse}(t) + C_{waste}(P_{NE}(t) - P_{NEuse}(t)) \tag{2}$$

In the formula, C_E represents the cost of new energy electricity bills; C_{waste} is the curtailment penalty cost; P_{NEuse} is for users to use new energy power; P_{NE} is the total power generated by new energy sources.

Based on Equations (1) and (2), the economic operating costs function is defined as the sum of the operating costs and the renewable energy utilization costs, shown as formula (3):

$$F_1 = C_a + C_b \tag{3}$$

Energy Storage Health Evaluation Function. To achieve efficient and stable long-term operation of the energy storage system, it is essential to holistically consider both the coordinated control of multiple devices and the individual health status of each unit. Therefore, we need to independently modeling each energy storage device in the system, establishing an energy storage health evaluation function to optimize and coordinate the output allocation between multiple devices and the operation instructions of a single device, thereby improving the service life of energy storage. This function mainly includes two indicators: the output indicator F_{ave} between collaborative energy storage devices and the indicator F_{wav} to prevent frequent charging and discharging of energy storage devices. In order to more intuitively demonstrate the effectiveness of the energy storage health evaluation function, the collaborative indicator and fluctuation indicator can be converted into the form of depreciation cost, directly reflecting their impact on energy storage health. As shown in formula (4):

$$F_2 = C_{bin} + C_{bw} + \alpha_1 F_{ave} + \alpha_2 F_{wav} \tag{4}$$

In the formula, C_{bin} is the initial investment cost of energy storage, C_{bw} is the maintenance cost of energy storage, F_{ave} is the energy storage synergy index, F_{wav} is the energy storage fluctuation index, α_1 is the energy storage synergy cost coefficient, and α_2 is the energy storage fluctuation cost coefficient.

Among these, the energy storage coordination index serves as a comprehensive parameter designed to quantify both the cooperative performance and overall operational effectiveness of multiple energy storage devices when functioning collectively. To prevent accelerated aging of individual energy storage devices caused by overcharging and overdischarging, additional penalties are imposed on devices whose state of charge deviates from the mean, as shown in formula (5):

$$F_{ave} = \sum_{t=1}^{T} \sum_{m=1}^{M} \left| S_{OC,ave}^{t} - S_{OC}^{t,m} \right| \tag{5}$$

In formula (5), m is the energy storage device number (total of M), $S_{OC,ave}^{m}$ is the average SOC of all energy storage devices during the t period; $S_{OC}^{t,m}$ is the SOC of the m-th energy storage device during the t time period.

The energy storage fluctuation index characterizes the dynamic variation patterns of either power output or state of charge (SOC) in energy storage devices when responding to power demand variations over time. To reduce the health loss caused by frequent charging and discharging of energy storage devices, a SOC fluctuation penalty function is introduced to suppress the rapid changes in the state of charge of each unit, as shown in formula (6):

$$F_{wav} = \sum_{t=1}^{T}\sum_{m=1}^{M}\left|S_{OC,ave}^{m} - S_{OC}^{t,m}\right| \tag{6}$$

In the formula, $S_{OC,ave}^{m}$ is the average SOC of the m-th energy storage device for the entire period of time.

The operational cost of energy storage systems comprises the initial capital investment cost C_{bin} and ongoing maintenance expenses C_{bw}, as shown in formula (7), where C_{bin} and C_{bw} are:

$$\begin{cases} C_{bin} = \sum_{m=1}^{M}(C_{p'}P_{m}^{'} + C_{E'}E_{m}^{'}) \\ C_{bw} = \sum_{m=1}^{M}(C_{w}P_{m}^{'}) \end{cases} \tag{7}$$

In the formula: $C_{p'}$ represents the cost of charging and discharging power for a single device; P'_m represents the rated power of the m-th device; $C_{E'}$ is the unit capacity cost; E'_m refers to the rated capacity of the m-th device; C_w is the annual maintenance cost for a single device.

In summary, a multi-objective optimization method is established that simultaneously considers economic benefits and energy storage health, as shown in formula (8):

$$\min(F) = \arg\min(F_1, F_2) \tag{8}$$

In the formula: F_1 is the system economic benefit function; F_2 is the energy storage health evaluation function.

2.2 Constraints

Power Balance Constraint. In order to ensure power balance between the electricity generated in the wind-solar-thermal-storage system and the load required by users, and to prevent situations of insufficient or excessive power supply, it is particularly important to establish power balance constraints. The power balance constraint is shown in formula (9):

$$P_N^t + P_{NEuse}^t + P_{dis_bat}^t = P_{cha_bat}^t + P_L^t \tag{9}$$

In the formula: P_N^t is the output of the unit at time t; P_{NEuse}^t corresponds to the output of new energy at time t, $P_{dis_bat}^t$ and $P_{cha_bat}^t$ are the discharge power and stored power of the energy storage device at time t, respectively, and only one of the two has a numerical value at the same time, and both are positive numbers; P_L^t is the user demand load at time t.

Ramp Rate Constraint. The operating power of each unit during operation needs to meet its maximum/minimum power limit to ensure safe and stable operation of the unit. The ramp rate refers to the maximum and minimum allowable rate of change in output power of the unit during adjacent time intervals within the scheduling period, with constraints as shown in equations (10) and (11):

$$P_i^{min} \le P_i \le P_i^{max} \tag{10}$$

$$r_i^{min} \le \left| P_i - P_i^0 \right| \le r_i^{max} \tag{11}$$

P_i represents the output of the i-th unit, while P_i^{min} and P_i^{max} represent its lower and upper output limits, respectively. This constraint ensures that the unit operates within a safe and stable power range. P_i^0 represents the

output of the t-th unit during the previous scheduling interval, r_i^{min} and r_i^{max} represent the changes in output power of the i-th unit, with a decrease and an increase, respectively. To avoid mechanical stress due to rapid adjustments and to safeguard system stability, the power output fluctuations are constrained within the range of [r_i^{min}, r_i^{max}].

Energy Storage Devices Constraint. In order to extend the service life of the battery as much as possible, it is necessary to set the battery's state of charge limit and charge discharge limit. The energy storage SOC needs to operate within a given range to ensure good operating conditions, while the energy storage power cannot exceed the maximum capacity, and the charging and storage power cannot exceed the limit power. The constraint conditions are shown in formula (12):

$$\begin{cases} P_{cha_bat}^{pre} < P_{cha_bat}^{t} \\ P_{dis_bat}^{t} \le P_{dis_bat}^{pre} \\ S_{OC\min} \le S_{OC}^{t} \le S_{OC\max} \end{cases} \tag{12}$$

In the formula, $P_{cha_bat}^{pre}$, $P_{dis_bat}^{pre}$ respectively represent the rated charging/discharging power of energy storage; S_{OC}^{t} is the state of charge of the energy storage device at time t; S_{OCmin} and S_{OCmax} represent the lower and upper limits of the state of charge. This constraint helps avoid deep charging/discharging, thereby effectively reducing the physical degradation of the energy storage unit.

In order to ensure the safe and stable operation of the wind-solar-thermal-storage system in the next scheduling cycle, the total charging amount of the energy storage battery during this scheduling cycle should be equal to the total discharging amount, and its constraint is shown in formula (13):

$$S(0) = S(T) \tag{13}$$

In the formula, T represents the entire scheduling cycle, $S(0)$ represents the state of charge of the energy storage device before the start of the scheduling cycle, and $S(T)$ represents the state of charge of the energy storage device after participating in the entire scheduling cycle.

3 MNSGAII Optimization Algorithm

3.1 Population Initialization Strategy based on Faure Sequence

The original NSGA-II algorithm adopts a random generation strategy for initialization to ensure the dispersion of the population in the search space. Although it helps to increase the exploration range of the solution space, it cannot guarantee the quality of the initial population and is prone to losing diversity. Therefore, in order to improve the uniformity of the initial solution distribution in the decision space, this paper uses the Faure sequence to initialize the population and maps the Faure sequence to the given search space [L_i, U_i]. The mapping formula is:

$$u_{i,j} = L_i + (U_i - L_i) \cdot F_{i,j} \tag{14}$$

Among them, $F_{i,j}$ represents the coordinate value of the i-th Faure point in the j-th dimension. Therefore, the individuals for initializing the population can be represented as:

$$x_i = (u_{i,1}, u_{i,2}, ..., u_{i,d}), i = 0, 1, ..., N-1 \tag{15}$$

d is the number of decision variables, i.e. the dimension of each individual x_i.

Fig. 1 compares the distribution of 100 initial particles generated by Faure sequence and random method in two-dimensional space. From the figure, it can be seen that the Faure sequence can effectively enhance the uniform distribution characteristics of the population in the solution space.

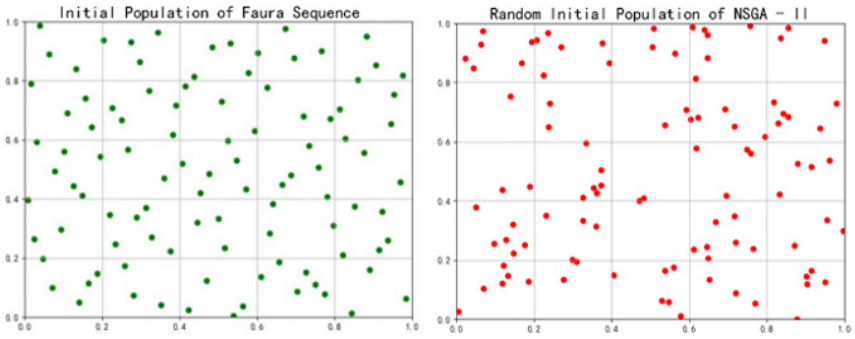


Fig. 1. Initialize population comparison chart

3.2 External Archive Mechanism

NSGA-II uses a dual layer selection mechanism of non dominated sorting and crowding distance sorting to retain non dominated solutions in the population, and selects individuals with better comprehensive performance in multiple objectives to enter the next generation of evolutionary process. During the iterative process of the algorithm, as the population continues to evolve, solutions in the boundary region of the Pareto front are easily eliminated, resulting in a reduction in the coverage range of the front; Secondly, in the absence of other effective mechanisms for enhancing diversity, selection pressure can lead to excessive concentration of solutions in certain high-density regions of the Pareto front in the population, resulting in uneven distribution of individuals in the target space. This concentration trend can significantly increase the similarity between individuals in the population, leading to a sharp decline in gene diversity and ultimately causing premature convergence problems.

Therefore, in order to fully search for potential optimal solutions and enhance the diversity of solutions, a dual archive strategy is proposed, with the core of simultaneously maintaining two independent archives, convergence archive and diversity archive. The specific strategy is as follows:

(1) Update strategy

a. Generate a set of reference vectors $W=(w_1, w_2,...,w_\mu)$ through uniform distribution, each vector representing a direction in the target space.

b. Each solution will be assigned to a specific subregion based on the angle between its objective function value and the reference vector, as shown in equation (16) [8]:

$$k(x) = \arg\min_{j\in\{1,...,\mu\}} \left\langle F(x), w_j \right\rangle \tag{16}$$

Among them, $F(x)$ is the normalized objective function value, and $\langle F(x), w_j \rangle$ is the angle between $F(x)$ and the reference vector w_j .

c. Using the boundary penalty crossover (PBI) value to measure the quality of solutions in each subregion, as shown in equations (17) to (19):

$$d_1(x) = \frac{|F(x)^T w|}{\|w\|} \tag{17}$$

$$d_2(x) = \left\| F(x) - d_1(x)\frac{w}{\|w\|} \right\| \tag{18}$$

$$PBI(x) = d_1(x) + \delta d_2(x) \tag{19}$$

Among them, $d_1(x)$ is the projection distance from $F(x)$ to w, $d_2(x)$ is the vertical distance from $F(x)$ to w, δ is a predefined penalty factor, $d_1(x)$ reflects the convergence of the solution along the reference vector direction, and the smaller the value, the closer it is to the Pareto front; $d_2(x)$ reflects the degree of deviation between the solution and the reference vector, with a smaller value indicating a more uniform spatial distribution of the solution. For each solution, store the solution with the smallest PBI value in the subregion in A_p, and the dominance relationship is shown in equation (20):

$$u \prec_{sp} v \Leftrightarrow PBI(u) < PBI(v) \tag{20}$$

d. Calculate the Manhattan distance between solution and solution A_p in the target space. If the distance between the current solution and all solutions in the archive is greater than a certain threshold, the solution will be stored in archive A_D.

e. In each generation of evolution, environmental selection relies on the information from these two archives: selecting the solution closest to the Pareto front from the convergence archive A_p; Selecting the solution with the widest distribution in the target space from the diversity archive A_D ensures that the algorithm not only considers convergence during each generation update process, but also preserves the diversity of the solution set through archive strategy.

(2) Truncation strategy

As the evolutionary process progresses, external archives will continue to accumulate high-quality solutions, leading to their continuous expansion in scale. To this end, an effective truncation mechanism needs to be established to screen individuals when they exceed the preset capacity, ensuring stable population size. The external archive truncation mechanism is as follows:

a. Merge archives A_p and A_D with the previous layer's non dominated solution $F(i\text{-}1)$ to form solution set P_{set}, sort P_{set} in a non dominated manner, and obtain a new population result $F'(i\text{-}1)$.

b. Determine whether the size of A_p and A_D meets the requirements. If $|A_p|+|A_D| \leq N$, it will be directly merged into the next generation subgroup; $|A_p|+|A_D| > N$, calculate the PBI values in $F'(i\text{-}1)$, select the first $N/2$ solutions in ascending order of PBI values, calculate the sparsity of solution A_D in the target co-construction using equation (21), sort in descending order of sparsity, and retain the first $N/2$ solutions.

$$d_{\text{Sparsity}}(x) = \min_{y \in A_d, y \neq x} D(x, y) \tag{21}$$

In the formula, x is the solution to be evaluated, y is the other solutions in archive A_D except for x, and $D(x, y)$ is the Euclidean distance between solutions x and y in the solution space.

To summarize, this dual-archive approach divides the search space into sub-regions, identifies the solution with the lowest PBI value in each for the convergence archive, and populates a diversity archive based on Manhattan distance metrics. By utilizing a truncation mechanism to manage archive capacity, the strategy maintains a robust trade-off between the convergence and diversity of the solution set during algorithm evolution.

3.3 MNSGA-II Algorithm Workflow

The overall steps of MNSGA-II are presented in Algorithm 1, and the flowchart is shown in Fig. 2.

Algorithm 1 :MNSGA-II algorithm

Input: N(external archive size),M(total polulation size),$Gen_{\max}$(maximum iterations),F_1, F_2, constraints

Output: Optimal compromise solution

Initialize population $P(t)$ using Faura sequence according to Equation (14) and (15)

Assign solutions of $P(t)$ to specific subspaces via Equation (16)

Generate the 1st generation subgroup via selection, crossover, mutation

Merge Parent and Offspring

for $Gen = 2$ **to** $Gen_{\max} - 1$ **do**

  while new parent population is not generated **do**

    Archive update mechanism

    Archive truncation mechanism

    Select individuals from A_p and A_D to generate a new parent population

    Merge Parent and Offspring

  end while

  Merge Parent and Offspring

  $Gen = Gen + 1$

end for

Extract non-dominated set PF

for all $x \in PF$ **do**

calculate its corresponding fuzzy membership function $\mu_j(x)$[9]

$$\mu_j(x) = \begin{cases} 1, & if : F_j(x) \le F_j^{\min} \\ \dfrac{F_j^{\max} - F_j(x)}{F_j^{\max} - F_j^{\min}}, & if : F_j^{\min} \le F_j(x) \le F_j^{\max} \\ 0, & if : F_j(x) \ge F_j^{\max} \end{cases}$$

Among them, $F_j^{\min}$ and $F_j^{\max}$ are the minimum and maximum values of the j-th objective function in the non-dominated solution set, respectively

end for

For each solution x, calculate its comprehensive membership degree $\mu(x)$:

$$\mu(x) = \frac{\sum_{j=1}^{m} \mu_j(x)}{\sum_{x \in PF} \sum_{j=1}^{m} \mu_j(x)}$$

Among them,m represents the number of objective functions, and PF represents the non dominated solution set.

Choose the solution with the highest comprehensive membership degree as the optimal compromise solution:

$$x^* = \arg\max_{x \in PF} \mu(x)$$

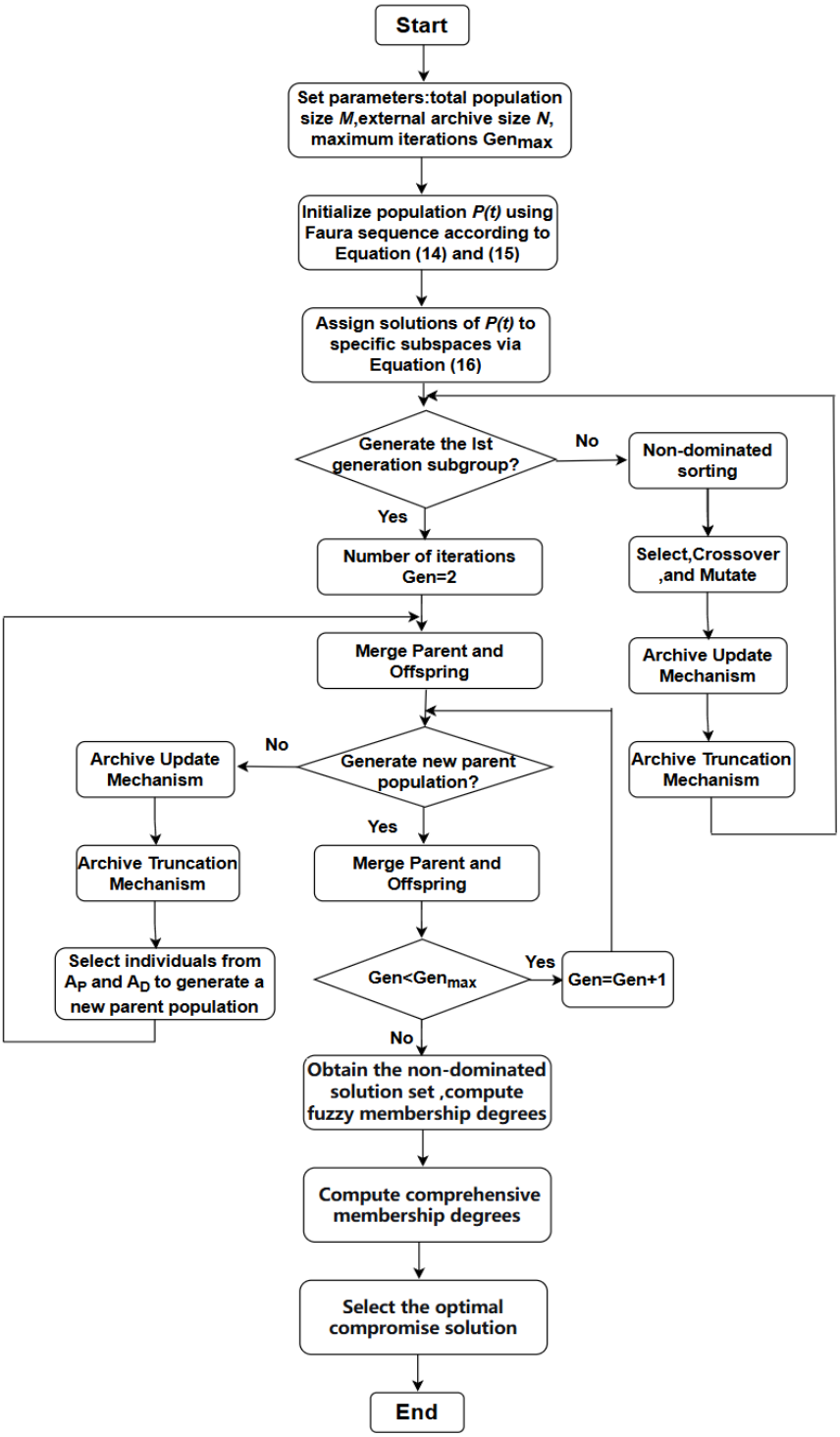


Fig. 2. MNSGA-II algorithm flowchart

Compared with the traditional NSGA-II, although MNSGA-II incurs a slight additional computational overhead due to the introduction of the dual-archive mechanism, its overall time complexity remains at $O(m\,M^2)$.

3.4 Experimental Analysis

Parameter Settings. The experiment is based on NREL's wind and solar power generation data and the required power load data of the system, and is equipped with 4 generator sets and 2 energy storage devices for research. The characteristic parameters of the adopted generator set are shown in Table 1: the second and third columns are the minimum and maximum output, respectively; columns 4 to 6 are the cost parameters of the unit during the power generation process; columns 7 and 8 are the power limits of the unit during the climbing process; columns 9 and 10 are the maximum and minimum start stop times of the unit.

Table 1. Characteristic parameters of generator units

Unit	P_{min}	P_{max}	a_i	b_i	c_i	P_{UR}	P_{DR}	T_S	T_G
1	30	100	34	1.7013	1.91	60	60	2	2
2	40	120	38	1.7526	1.97	60	40	3	3
3	40	140	27	1.7998	1.06	80	50	3	3
4	70	300	70	1.6055	1.31	150	90	5	5

To achieve effective regulation of the peak valley load difference in the power grid, energy is stored during valley periods and released during peak periods, reducing operational problems caused by excessive peak valley differences and ensuring stable operation and power quality of the power grid. The total installed capacity of energy storage is 100MW/80MWh, and the parameters are shown in Table 2:

Table 2. Energy storage parameters

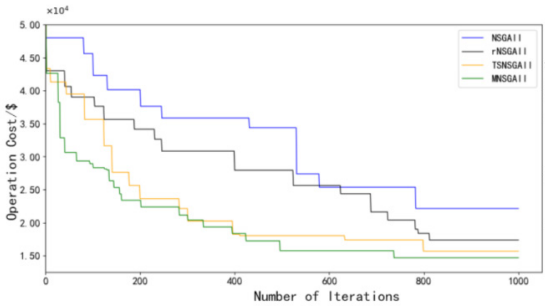
Parameter	Energy storage 1	Energy storage 2
Rated Power (MW)	50	50
Rated Capacity (MWh)	30	50
Unit Capacity Cost ($/kWh)	1000	1500
Unit Power Cost ($/kW)	1000	1000
Maximum Cycle Life (times)	3000	4500
Initial State of Energy Storage	0.5	0.5
SOC Range	[0.1, 0.9]	[0.1, 0.9]

Analysis of Scheduling Strategy Solution. In testing the multi-objective optimization model, the proposed MNSGA-II algorithm will be benchmarked against NSGA-II [10], rNSGA-II [11], and TS-NSGA-II [8]. In order to ensure fairness in the experiment, the population size of each algorithm is set to 50, the size of the archive is set to 50, the number of iterations is set to 1000, the scheduling period is set to 24 hours, and the time interval is set to 1 hour.

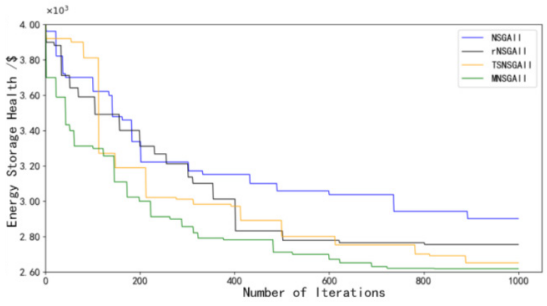
Fig. 3 shows a comparison of the optimal iteration curves of four algorithms on two optimization objectives. Among them, (a) represents the iterative curve of the power generation cost target, and (b) represents the iterative curve of the energy storage health target. Due to the iterative process relying solely on non dominated sorting strategies, the original NSGA-II lacks local search capabilities and is prone to getting stuck in local optima, resulting in the worst performance among the four algorithms. Due to the guidance of reference points in the early stage, the population of rNSGA-II converges quickly. Therefore, rNSGA-II can quickly search for regions in the early stage of iteration, and its performance is better than NSGA-II. However, it lacks the ability to search for local regions. TS-NSGA-II can use a two-stage update strategy in iterations, where individuals avoid local optima by transforming the update strategy. Compared to NSGA-II and rNSGA-II, TS-NSGA-II can detect better areas. Because the particles in MNSGA-II update their external archives through a dual archive mechanism during the iteration process, each generation of the population can learn from better particles, providing sufficient guidance particles during both the early and final search stages, and possessing excellent global search capabilities.

Table 3. Scheduling strategy of MNSGA-II

Time	P_1	P_2	P_3	P_4	P_w	P_p	P_{sc}	P_{load}
1	30	40	40	207	115	0	-34	398
2	35	45	45	185	142	0	0	452
3	40	50	50	177	125	0	0	442
4	50	60	60	186	125	0	0	481
5	60	70	70	103	120	0	60	483
6	70	80	80	122	115	0	0	467
7	80	90	90	107	130	25	-40	482
8	48	42	40	133	149	88	0	500
9	99	102	120	283	165	106	0	875
10	80	62	87	195	48	128	40	640
11	80	100	120	128	180	138	0	746
12	70	90	110	110	140	145	-55	610
13	60	80	100	103	138	148	-11	618
14	50	70	90	72	111	145	0	538
15	40	60	77	87	5	138	26	433
16	30	50	70	89	113	128	0	480
17	40	60	80	204	140	116	0	640
18	50	70	90	120	105	80	0	515
19	60	80	100	369	49	13	54	725
20	70	90	110	227	11	0	0	508
21	80	100	120	86	141	0	-40	487
22	90	110	130	82	68	0	0	480
23	100	120	140	80	58	0	0	498
24	90	110	130	70	23	0	0	423



(a) The iterative curve of the power generation cost target



(b) The iterative curve of the energy storage health target

Fig. 3. The iteration curves of four algorithms on two objectives during the iteration process

Fig. 4 shows the Pareto front solution sets of four algorithms. It can be seen from the figure that MNSGA-II has the best Pareto front, and MNSGA-II can ensure that both objectives reach a high level, rather than simply sacrificing on one objective. This means that MNSGA-II is more competitive than the other three algorithms in solving the scheduling problem in this paper, and can avoid obvious disadvantages in other objectives while ensuring accuracy.

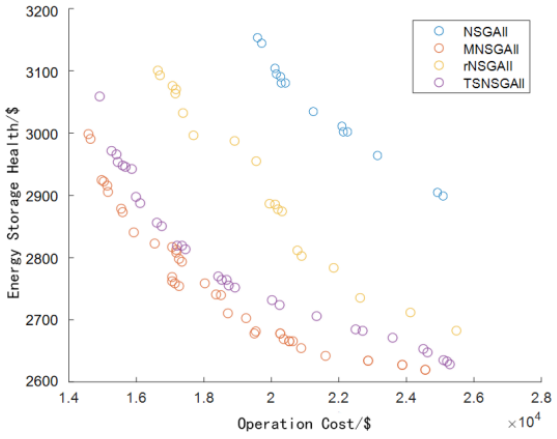


Fig. 4. Comparison of Pareto frontiers of algorithms

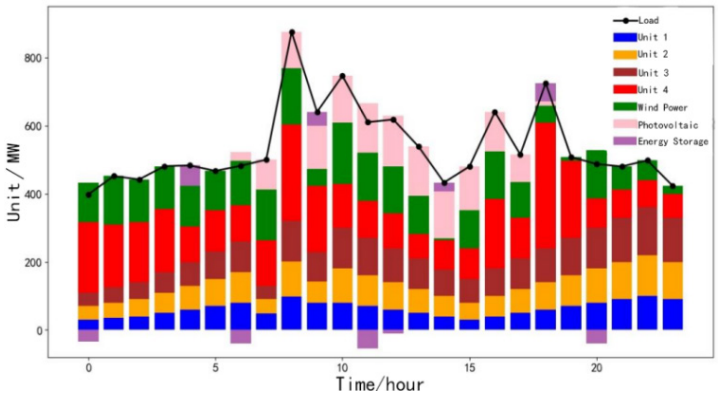


Fig. 5. Power constraint balance verification

To verify the correctness of the solution, Table 3 provides the scheduling strategy for the MNSGA-II algorithm. In the table, P_1, P_2, P_3, and P_4 represent the output of four units, P_w represents the output of wind power, P_p represents the output of photovoltaics, P_{sc} represents the overall output of two energy storage units, and P_{load} represents the required load of the system. Fig. 5 verifies that the scheduling strategy satisfies the power balance constraint. The stacked column chart represents the sum of the output power of each generator unit in each time period of the scheduling cycle. The output power of each unit in each scheduling cycle is represented by histograms of different colors. From the graph, it can be seen that the energy storage charging and discharging situation and the sum of the output power of each unit in each scheduling cycle are equal to the sum of the power load demand, indicating that the scheduling strategy obtained by the MNSGA-II algorithm meets the power balance constraint conditions. Fig. 6 shows the net load and output curve of the unit.

In summary, during the scheduling period, the output and energy storage of different units in each time period satisfy formulas (9) to (13). When the net load demand during different scheduling periods is similar, significant differences in unit output may still occur. This phenomenon is mainly due to two factors: first, the output of the unit has a time coupled characteristic, and the output decision of the current period must consider

the output status of the previous period; Secondly, the operation of the unit is limited by physical constraints such as climbing rate. Therefore, even if the net load of the system does not change significantly, there may still be significant differences in the actual output plan of the unit.

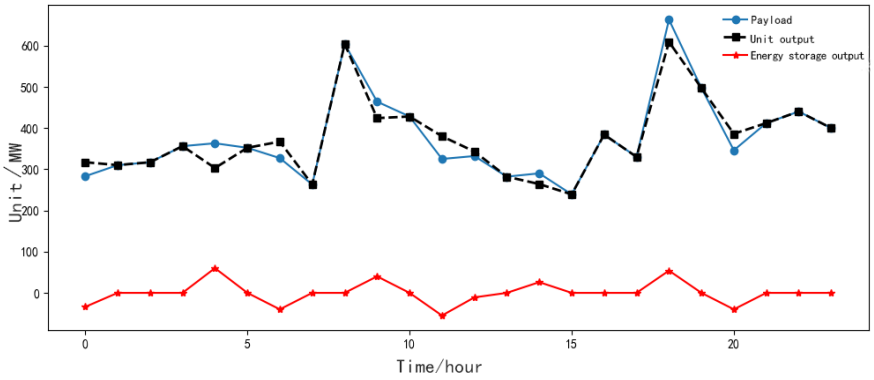


Fig. 6. Net load and output curve of the unit

4 Conclusion

In this paper, an enhanced MNSGA-II algorithm is developed in response to the limitations of traditional NSGA-II in local optima stagnation and poor diversity within multi-objective power dispatch. By employing Faure sequence-based initialization, the algorithm improves the uniformity of initial solution sets. A novel dual-archive mechanism, leveraging PBI and Manhattan distance metrics, is implemented to maintain a superior trade-off between convergence and diversity. Experimental results demonstrate that in a dispatch case study involving four generating units, MNSGA-II significantly outperforms the traditional NSGA-II and its variants in terms of Pareto front distribution, optimization precision, and convergence speed. Crucially, the generated dispatch strategies fully satisfy constraints such as power balance, generator ramp rates, and the physical characteristics of energy storage, offering an efficient and robust solution for the optimal scheduling of modern power systems under complex constraints.

Although this research has made some achievements, it still needs to explore the following aspects in the future:

(1) Expand from day ahead scheduling to rolling optimization and real-time scheduling within the day, and build a multi time scale coordination and optimization framework;

(2) Explore the deep integration of artificial intelligence and traditional optimization algorithms to further enhance the economy and reliability of scheduling schemes.

5 Acknowledgement

This work was supported by the Scientific Research Project of the Education Department of Jilin Province (JJKH20250880KJ).

References

[1] X. Wang, S. Li, Multi-Objective Optimal Scheduling of Microgrid Based on Improved Harris Hawks Optimization Algorithm, Distributed Energy 10(1)(2025) 91-100. https://doi.org/10.16513/j.2096-2185.DE.(2025)010-01-0091-10

[2] X.-L. Zhu, X.-Z. Guo, Multi-objective optimization strategy of islanding microgrid based on improved NSGA-II

algorithm, Journal of Physics: Conference Series 2450(1)(2023) 1-8.
https://doi.org/10.1088/1742-6596/2450/1/012092

[3] Z.-H. Wang, T. Wang, Q.-F. Niu, J.-F. Wu, M.-W. Li, S.-Q. Zhu, Research on multiobjective capacity configuration optimization of grid-connected wind–solar–storage microgrid system based on improved BWO algorithm, Energy Science Engineering 12(6)(2024) 2365-2384.
https://doi.org/10.1002/ese3.1727

[4] Z. Guan, H. Wang, Z. Li, X.-H. Luo, X. Yang, J.-G. Fang, Q. Zhao, Multi-Objective Optimal Scheduling of Microgrids Based on Improved Particle Swarm Algorithm, Energies 17(7)(2024) 1-20.
https://doi.org/10.3390/en17071760

[5] K. Deb, A Pratap, S. Agarwal, T. Meyarivan, A fast and elitist multiobjective genetic algorithm: NSGA-II, IEEE Transactions on Evolutionary Computation 6(2)(2002) 182-197.
https://doi.org/10.1109/4235.996017

[6] A. Hazra, M.-K Manna, A. Ganguly, R. Naska, A. Roy, Economic and Green Dispatch in Multi-Area Power Systems: An Approach of using NDSGA-II, International Journal of Communication, Science and Technology 1(3)(2025) 7-15.
https://www.jctmg.in/wp-content/uploads/2025/06/IJCST-V1I3-2506-012-1.pdf

[7] J. Liu, T.-X. Ding, T. Du, J. Du, Y. Zhang, Z.-Q. Bai, L.-H. Yang, F. Chen, The Economical Dispatch Model for Industrial Parks Considering the Lifetime of Energy Storage Batteries, Power System and Clean Energy 40(5)(2024) 105-112.
https://doi.org/10.3969/j.issn.1674-3814.2024.05.013

[8] F. Ming, W.-Y. Gong, L. Wang, A two-stage evolutionary algorithm with balanced convergence and diversity for many-objective optimization, IEEE Transactions on Systems, Man, and Cybernetics: Systems 52(10)(2022) 6222-6234.
https://doi.org/10.1109/TSMC.2022.3143657

[9] M.A. Abido, Environmental/economic power dispatch using multiobjective evolutionary algorithms, IEEE Transactions on Power Systems 18(4)(2003) 1529-1537.
https://doi.org/10.1109/TPWRS.2003.818693

[10] S.-S. Shi, Y. Zhang, Z.-J. Fu, C. Fang, Y.-F. Wang, L.-Y. Zhao, Optimal Configuration of Energy Storage System Capacity in PV-integrated EV Charging Station Based on NSGA-III, Journal of Physics: Conference Series 1993(1)(2021) 1-10.
https://doi.org/10.1088/1742-6596/1993/1/012013

[11] E. Filatovas, A. Lančinskas, O. Kurasova, J. Žilinskas, A preference-based multi-objective evolutionary algorithm R-NSGA-II with stochastic local search, Central European Journal of Operations Research 25(4)(2017) 859-878.
https://doi.org/10.1007/s10100-016-0443-x